Graphical Table of Contents

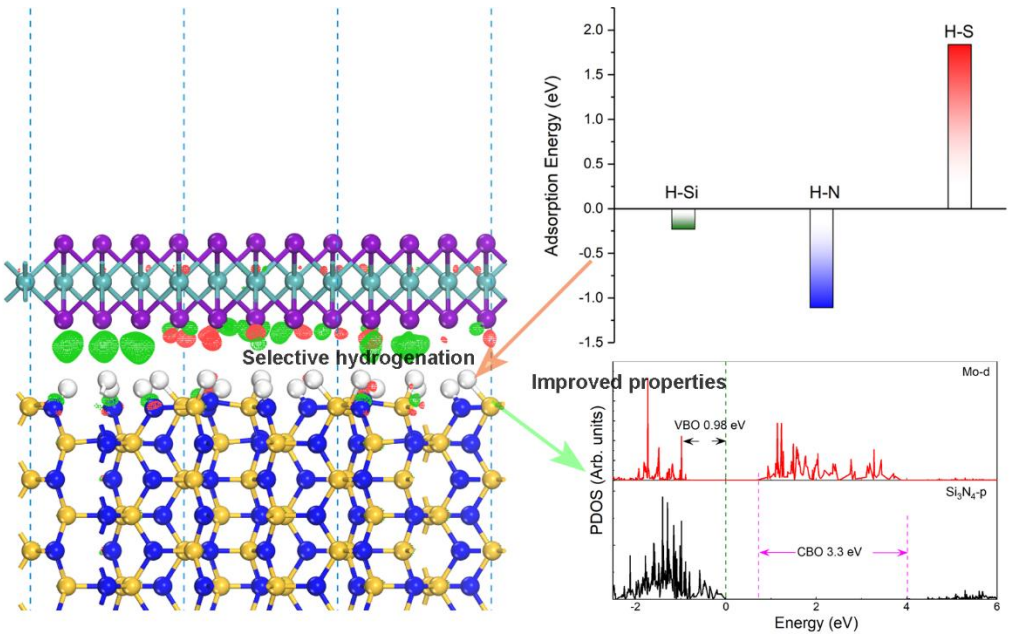

The hydrogenation process can selectively passivate the interface states at the high-*k* dielectrics while does not affect the 2D semiconductors, enabling an improved integration of high-*k* dielectrics on 2D materials based nanoelectronics.

Selective hydrogenation improves interface properties of high-*k* dielectrics on 2D semiconductors

Yulin Yang[1, #], Tong Yang[2, #], Tingting Song[3], Jun Zhou[4], Jianwei Chai[4], Lai Mun Wong[4], Hongyi Zhang[1], Wenzhang Zhu[1], Shijie Wang[4, *], and Ming Yang[2, *]

[1] Fujian Provincial Key Laboratory of Optoelectronic Technology and Devices, School of Optoelectronic and Communication Engineering, Xiamen University of Technology, Xiamen, 361024, China

[2] Department of Applied Physics, The Hong Kong Polytechnic University, Hung Hom, Kowloon, Hong Kong SAR, China

[3] College of Physics and Space Science, China West Normal University, Nanchong, 637002, China

[4] Institute of Materials Research and Engineering, Agency for Science, Technology and Research (A*STAR), 2 Fusionopolis Way, Innovis, 138634, Singapore

[#] These authors contributed equally to this work.

[*] Author to whom correspondence should be addressed: M.Y. (mingyang@polyu.edu.hk) or S.J.W. (sj-wang@imre.a-star.edu.sg)

Abstract

The integration of high-*k* dielectrics with two-dimensional (2D) semiconductors is a critical step towards high-performance nanoelectronics, which however remains challenging due to high density of interface states and the damage to the monolayer 2D semiconductors. In this study, we propose a selective hydrogenation strategy to improve the interface properties while the 2D semiconductors are not affected. Using the interface of monolayer MoS_2 and silicon nitride as an example, we show substantially improved interface properties for electronic applications after the interfacial hydrogenation, as evidenced by reduced inhomogeneous charge redistribution, increased band offset, and nearly intact electronic properties of MoS_2. Importantly, this hydrogenation process selectively occurs only at the silicon nitride surface and is compatible with the current semiconductor fabrication process. We further show that this strategy is general and applicable to other interfaces between high-*k* dielectrics and 2D semiconductors such as HfO_2 on the monolayer MoS_2. Our results demonstrate a *simple yet viable* way to improve the integration of high-*k* dielectrics on a broad range of 2D transition metal disulfide semiconductors, shedding light on practical electronic and optoelectronic applications.

Keywords

Two-dimensional materials, high-*k* dielectrics, molybdenum disulfide, interfacial properties, transition metal disulfide

Introduction

Two-dimensional (2D) semiconducting materials are appealing for nanoelectronic applications in the post-Moore era as their ultra-thin thickness can help to minimize the short channel effect confronted with current Si based technologies.[1, 2] Among them, monolayer transition metal disulfides (TMDs) such as MoS_2 and WS_2 have attracted tremendous interest as promising channel materials for electronic or optoelectronic devices due to their stability, direct band gaps, tunable electronic and optical properties, and many other excellent physical properties[3-13] The monolayer MoS_2 based nanotransistors have shown encouraging device performance such as a high on/off ratio.[14-16] However, to utilize monolayer TMDs in practical electronic applications, there remain many challenges[17], which include the large-scale growth of high-quality TMDs layers [18-22], metal contact with low resistance[23-28], and the integration of high-*k* dielectrics.[29-32]

In particular, for electronic applications, the integration of high-*k* dielectrics is highly desired as their large dielectric constants can effectively screen the scattering from charge impurities and thus improve the device performance.[33, 34] However, it is found difficult to achieve high-quality interfaces between high-*k* dielectrics and monolayer TMDs due to high interface state density.[31, 32] Currently, a high-quality interface can be realized by van der Waals (vdW) integration of *h*-BN or CaF_2 layers on TMDs semiconductors.[35-37] However, recent studies show a high leakage current in the 2D electronic devices using *h*-BN as the dielectric, impeding its practical application as the gate dielectric in ultrascaled nanoelectronics.[38] Besides, the integration strongly relies on the transfer process, which is challenging to be scaled up for large-scale practice applications. While various attempts have been made to directly deposit high-*k* oxides such as $HfO_{2[39]}$, $Al_2O_{3[40, 41]}$ and $ZrO_{2[42]}$ on TMDs layers using atomic layer deposition (ALD) or sputtering technique, their interfacial properties are still much inferior to that of HfO_2/Si and need further improvement.[32, 43]

One such endeavor is interface engineering, which includes interface passivation by annealing [44, 45], and utilizing interface seeding or buffer layers[31, 32, 46]. These strategies have brought some improvement from their respective effects but may also raise new problems such as the damage of the 2D TMDs semiconductors and accordingly deteriorated electronic properties. [31, 32] Thus, it is highly desirable to develop a holistic strategy that can effectively passivate the interfacial dangling bonds of high-*k* dielectrics and also protect the 2D semiconductors. In this study, we propose selective hydrogenation as such an ideal strategy, due to that the hydrogen atoms are prone to be adsorbed on the surface of high-*k* dielectrics but inert to the basal planes of 2D TMDs. We use the interface between monolayer MoS_2 and β-Si_3N_4 (0001) as an example to deliver the concept and apply this strategy to another interface between MoS_2 and HfO_2 to demonstrate its generality.

1. Method

All the calculations were performed using density-functional theory (DFT) based the Vienna Ab initio Simulation Package (VASP.5.4.4.18) with the Perdew-Burke-Ernzerhof (PBE) functional and the projector-augmented wave (PAW) potentials.[47-49] The cutoff energy for the plane wave expansion was set to 500 eV. Γ-centered 9×9×4, 12×12×1, 6×6×1, and 9×9×1 *k*-point meshes were used to sample the first Brillouin zone of bulk β-Si_3N_4, monolayer MoS_2, and the interface of monolayer MoS_2 on β-Si_3N_4 (0001) and *c*-HfO_2 (111), respectively. A vacuum layer with a thickness of 15 Å was used for all slab structures to minimize the artificial Coulomb interaction between two adjacent surfaces. For the interface structures, the vdW correction has been included by Grimme's DFT-D3 method.[50] For all calculations, the electronic and ionic convergence criteria were set to 10^{-5} eV and 0.01 eV/Å, respectively. The lattice constants are calculated to be a=b=7.659 Å and c=2.925 Å for β-Si_3N_4 and a=b=3.184 Å for monolayer MoS_2, and the corresponding PBE band gaps are 4.24 eV and 1.66 eV, respectively. All these results are well consistent with previous studies.[51-55]

The interface structures were constructed by placing the (4×4×1) monolayer MoS_2 supercell on the ($\sqrt{3}\times\sqrt{3}\times1$) β-Si_3N_4 (0001) surface without/with surface hydrogen passivation, in which a 3.97% compressive strain was applied to the Si_3N_4. This strain yields a reduced PBE band gap by ~0.2 eV in the Si_3N_4 (see Fig. S1 in the Supporting Information), while the main electronic structure does not change much compared with that of the pristine bulk Si_3N_4. The thickness of the β-Si_3N_4 (0001) surface was set to 7 atomic layers, the bottom layer of which was passivated using hydrogen atoms. In the interface structures, dipole correction was applied.[56] To examine interfacial stability of monolayer MoS_2/hydrogen passivated β-Si_3N_4 (0001), *ab initio* molecular dynamics simulations were performed on the interface supercell, where the canonical ensemble (NVT) and the Nosé heat bath were adopted with a time step of 1 fs and a time length of 6 ps

The interfacial interaction strength between monolayer MoS_2 and dielectrics (D, Si_3N_4 or HfO_2) can be estimated from the adsorption energy (E_{ad}) as defined below:

$$E_{ad} = \frac{E_{\mathrm{MoS_2}+D} - E_{\mathrm{MoS_2}} - E_D}{A}, \quad (1)$$

where $E_{\mathrm{MoS_2}+D}$ is the total energy of the hybrid interface structure for MoS_2 on the dielectrics, E_{MoS_2} and $E_D$are the total energy of the isolated MoS_2 monolayer and the dielectric (Si_3N_4 or HfO_2) surface, respectively, and A is the interface area. Similarly, the charge redistribution $\Delta\rho$ for MoS_2 monolayer on the dielectric surface is defined as:

$$\Delta\rho = \rho_{\mathrm{MoS_2}+D} - \rho_{\mathrm{MoS_2}} - \rho_D, \quad (2)$$

in which $\rho_{\mathrm{MoS_2}+D}$ is the charge density of the hybrid interface structure for MoS_2 on the dielectric, and $\rho_{\mathrm{MoS_2}}$ and $\rho_D$are the charge density of the isolated MoS_2 monolayer and the dielectric (Si_3N_4 or HfO_2) surface, respectively.

2. Results and discussions

Silicon nitride (Si_3N_4) has a large band gap and high thermal stability, which has been widely applied in current Si based electronic devices.[53, 54, 57] It was reported that high-quality Si_3N_4 thin films can be deposited on graphene[52, 58, 59], while the electronic properties of the latter does not change much. [58] Furthermore, Si_3N_4 might be a better choice than the metal oxides as a high-*k* dielectric because it does not contain metallic ions which tend to interact strongly with 2D TMDs.[51, 60, 61] Thus, in this study, we use the interface between monolayer MoS_2 and β-Si_3N_4 as a model example to study the hydrogenation effect on the interface properties.

We have constructed various interface structures by sliding the MoS_2 on the Si_3N_4 surface. The energy difference among these configurations is within 12 meV (see Fig. S2(a)), inferring a weak interfacial interaction. The top and side view of the most stable interface configuration is shown in Fig. S2(b) and Fig 1(a), respectively, in which the interfacial S atoms of MoS_2 tend to arrange near the interfacial Si atoms of Si_3N_4 to maximize the potential bonding. Similar trend has been reported at the MoS_2/HfO_2 and high-*k* dielectrics/graphene interfaces.[51, 62, 63] The interface spacing between monolayer MoS_2 and β-Si_3N_4 (0001) is about 2.9 Å, at the lower bound of the vdW interaction range, further indicating weak interface interaction. The interface interaction strength can also be measured from the adsorption energy (-23.2 meV/Å^2). This value is slightly higher than that of bi-layer MoS_2 (-22.4 meV/Å^2), but it is much smaller than those of other high-k dielectric/TMDs interfaces such as MoS_2/HfO_2 and MoS_2/SiO_2.[51, 61, 64]

The projected density of states (PDOSs) of monolayer MoS_2 on β-Si_3N_4 (0001) is shown in Figs. 1(c-e). One important observation is that the electronic structure of monolayer MoS_2 is nearly intact in the presence of the Si_3N_4 due to relatively weak interaction between

them. As the PDOS shown in Fig. 1(c), the monolayer MoS_2 remains semiconducting with a PBE gap of ~1.6 eV. This is highly desired because a sizable band gap in semiconductors enables a stable device operation with a large on/off ratio. However, due to the dangling bonds in β-Si_3N_4 (0001) (see Fig. S3) induced mid-gap states, orbital hybridization is seen between MoS_2 and Si_3N_4. As Figs. 1(b-d) show, the Mo e_g orbitals couple with the p orbitals of Si and N ions near the valence band edge, while at the conduction edge, the hybridization among Mo e_g, S p_z orbital and Si p_z orbital is more noticeable. This orbital hybridization leads to insignificant band offsets between MoS_2 and Si_3N_4, which is unfavorable for device applications. To minimize the tunneling current in semiconductor devices, the valence and conduction band offset between the semiconductor (e.g., MoS_2 in this study) and the gate dielectric (e.g., Si_3N_4 here) should be larger than 1 eV.[33] In addition, the interfacial interaction causes charge redistribution at the interface (see Fig. 1(a)), where the accumulated charges are closer to Si_3N_4 surface while the depleted charges are more pronounced near MoS_2 side. The charge redistribution induces electron-hole puddles in monolayer MoS_2, as shown in Fig. 1(b). This is another detrimental effect for electronic device applications as the electron-hole puddles can be charge scattering centers which reduce the carrier mobility.[65]

Since the degraded interface properties are mainly due to the dangling bonds at the β-Si_3N_4 (0001) surface, one natural attempt for improving the interface properties is to passivate them. We note that the hydrogenation process has been widely used in semiconductor technologies to passivate the intrinsic defects.[66] Such process may also be applied to passivate the dangling bonds of the β-Si_3N_4 (0001) surface considered in this study. After passivation (see the atomic structures in Fig. S4(a)), the dangling bonds induced states nearly vanish as confirmed by the PDOSs in Fig. S4(b). Consequently, the interfacial interaction between monolayer MoS_2 and hydrogen passivated β-Si_3N_4 (0001) surface is further weakened. The calculated adsorption energy (see Fig. 2(a)) decreases slightly to -18.2 meV/Å^2. The charge

redistribution is shown in Fig. 2(b) and (c), which clearly suggests that the weaker interfacial interaction results in much less pronounced interfacial charge redistribution, as well as the suppressed electro-hole puddles in the Mo atomic plane.

After the hydrogen passivation on the β-Si_3N_4 (0001) surface, the orbitals near Fermi level between monolayer MoS_2 and Si_3N_4 are well separated. From Fig. 2(d), we can see that the valence band edge now is contributed by p orbital from Si_3N_4, while the states contributed by Mo d orbital are located at -0.98 eV below the Fermi level. In contrast, the conduction band edge is mainly derived from Mo d orbital, and the contribution from p orbital of Si_3N_4 starts from ~4.88 eV and above. This leads to a type-II band offset between monolayer MoS_2 and Si_3N_4, in which the valence band (VBO) and conduction band offset (CBO) can be estimated to be 0.98 and 3.3 eV at the PBE level (see Fig. S5), respectively. It should be noted that these band offset values might be underestimated, which could be larger if the quasiparticle corrections or hybrid functionals are used. With the hydrogen passivation, we also find improvement on the electronic properties of monolayer MoS_2. As shown in Fig. 2(e), the electronic structure of monolayer MoS_2 on the hydrogen passivated Si_3N_4 is nearly identical to that of free-standing monolayer MoS_2. Thus, we can see that using this simple hydrogenation process, the interface properties of MoS_2/Si_3N_4 are improved remarkably as evidenced by the large band offsets, suppressed electron-hole puddles, and intact electronic properties of MoS_2.

More importantly, the hydrogenation process is energetically selective to β-Si_3N_4 (0001) surface. As shown in Fig. 3(a), the adsorption energy for hydrogen atom on top of Si site at the Si_3N_4 surface is -0.23 eV, and the lowest adsorption energy on the top of the N sites is -1.11 eV due to the dangling bonds of N ions at the surface. The negative adsorption energy indicates that the hydrogen adsorption is energetically favorable, and the hydrogenation can occur spontaneously even at a low temperature. In contrast, the energy for hydrogen atoms adsorbed on the monolayer MoS_2 is calculated to be 1.84 eV, consistent with previous studies.[67] The

large positive adsorption energy suggests that the hydrogenation on the monolayer MoS_2 is energetically unfavorable, which is less likely to happen even at a high processing temperature. Further quantum mechanical molecular dynamics simulation shows that the hydrogen passivated MoS_2/Si_3N_4 interface is thermodynamically stable at the high temperature of 800 K. From Fig. 3(b) and Fig. S(6), it is noted that the variation of interfacial Si-H and N-H bond length is within 0.2 Å during the MD simulation, suggesting that the Si_3N_4 surface adsorbs hydrogen atoms so strongly that they are unlikely to diffuse to monolayer MoS_2 even at the temperature of 800 K (see Fig. 3(c)). This implies that the spontaneously selective hydrogenation process is compatible and stable with current semiconductor device fabrication processes, as most of them are conducted below 800 K.[68]

Next, we show that the hydrogenation process is applicable for improving interface properties of other high-*k* oxides and monolayer MoS_2. Since HfO_2 has been widely used in current electronic devices, we use it as a model example to further examine the hydrogenation effects. It has been reported that Hf-terminated HfO_2 interacts strongly with MoS_2, leading to inferior electronic properties, while the interface between O-terminated HfO_2 and MoS_2 shows improved interface performance.[51] Thus, we focus on the interface of Hf-terminated HfO_2 and monolayer MoS_2 without/with the interfacial hydrogenation. As Figs. 4(a) and (c) show, at the interface of Hf-terminated HfO_2 and monolayer MoS_2, it forms interfacial covalent Hf-S bonds. This induces noticeable charge transfer from HfO_2 into MoS_2, making the MoS_2 metallic. Similarly, the interface properties can be improved using the hydrogenation process. Figures 4(b) and (d) are the charge redistribution and local density of states (LDOS) for monolayer MoS_2 on the hydrogen passivated Hf-HfO_2 (0001) surface, respectively. The reduced interfacial charge redistribution and the suppressed mid-gap metallic states in MoS_2 clearly suggest that better interface properties are reached by the selective hydrogen passivation.

It has been noted that 2D materials with HfO_2 thin films grown by atomic layer deposition (ALD) technique show better device performance than those using sputtering or physical vapor deposition (PVD).[69] We argue that the underlying mechanisms, in addition to the film uniformity and quality, could be partially ascribed to unintended hydrogen passivation on the high-*k* oxide film. In ALD process, the Hf metal-based precursor and water vapor are used for the deposition of HfO_2[70], in which residual hydrogen source[71] might evolve to passivate the dangling bonds, whereas the high vacuum required in sputtering or PVD process leads to negligible residual hydrogen sources. Thus, we expect that the interface between high-*k* dielectrics and MoS_2 can be further improved by intentionally depositing the high-*k* dielectric films in the hydrogen environment at the first few cycles. Please note that the effectiveness of this interfacial hydrogenation strategy is strongly dependent on the difference in the hydrogen adsorption on 2D materials and high-*k* dielectrics. If hydrogen interacts strongly on the 2D materials such as graphene[72] or phosphorene[73], the hydrogenation process would result in undesired hydrogen adsorption on the 2D materials, leading to considerable changes in the electronic properties of 2D materials. On the contrary, as long as a 2D material is unfavorable to bind hydrogen, the hydrogenation process proposed here is beneficial to its integration with high-*k* dielectrics. The beneficial effects of this hydrogenation strategy on the interface integration are two-folds: one is to passivate the dangling bonds in the high-*k* dielectrics, resulting in reduced interface state density; the other is to passivate the native defects in 2D TMDs, which improve electronic properties of the 2D semiconductors, as supported by the electronic structure (see Fig. S7) of monolayer MoS_2 with/without the hydrogen passivation on the S vacancies.

3. Conclusions

In conclusion, we report a simple yet effective strategy to improve the interfacial properties of high-k dielectrics and 2D semiconductors, as supported by the substantially

improved electronic properties at the interface between Si_3N_4 and monolayer MoS_2 using the proposed selective hydrogenation process. This hydrogenation process spontaneously occurs on Si_3N_4, leaving the monolayer MoS_2 nearly intact. We reveal that the hydrogenated MoS_2/Si_3N_4 interface is stable at high temperatures, which is compatible with the current semiconductor fabrication process. We further show that the interfacial hydrogenation strategy can be applied for the integration of other high-*k* dielectrics on MoS_2 monolayer. Given similar surface chemistry among TMD semiconductors, this hydrogenation process can be extended to the interfaces of many high-*k* dielectrics and a broad range of transition metal disulfides such as MoS_2, WS_2, or HfS_2, as well as some transition metal dichalcogenides such as $MoSe_2$ or WSe_2, or other 2D materials that are inert to hydrogen adsorption, enabling us to boost the development of 2D semiconductors based nanoelectronic devices.

Acknowledgements

M.Y. acknowledges the funding support (project IDs: 1-BE47 and ZE2F) from The Hong Kong Polytechnic University. We acknowledge Centre for Advanced 2D Materials and Graphene Research at National University of Singapore, and the National Supercomputing Centre of Singapore for providing computing resources.

Conflict of Interest

The authors declare no conflict of interest.

Electronic Supplementary Material: Supplementary material (DOS of bulk β-Si_3N_4; Relative stability of interface configurations; DOS of β-Si3N4 surface; DOS of hydrogen passivated β-Si_3N_4 surface; Band alignment; N-H bond variations; Electronic structures of monolayer MoS_2 with a S vacancy before and after passivation) is available in the online version of this article at http://dx.doi.org/10.1007/**********.

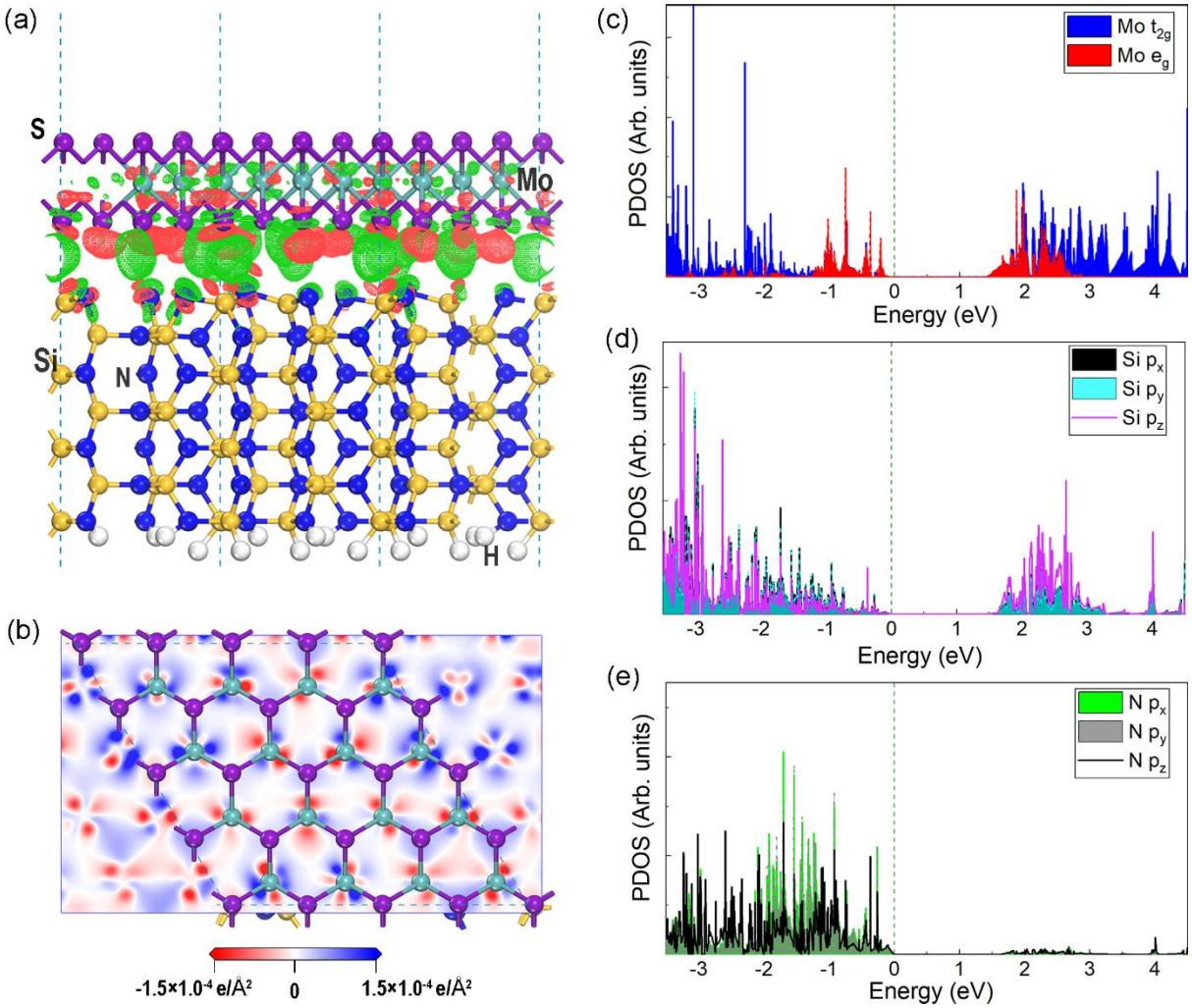

Figure 1. Interface properties between monolayer MoS_2 and β-Si_3N_4 (0001). (a) side and (b) top view of the most stable configuration for monolayer MoS_2 on β-Si_3N_4 (0001), in which the red and green dots in (a) denote the depleted and accumulated charge density visualized by an iso-surface value of 1.5×10^{-4} e/Å^3, respectively. The red and blue colour in (b) denotes charge puddles on the Mo plane. The projected density of states (PDOSs) for Mo (c), Si (d) and N (e), where the Fermi level is set to 0 eV.

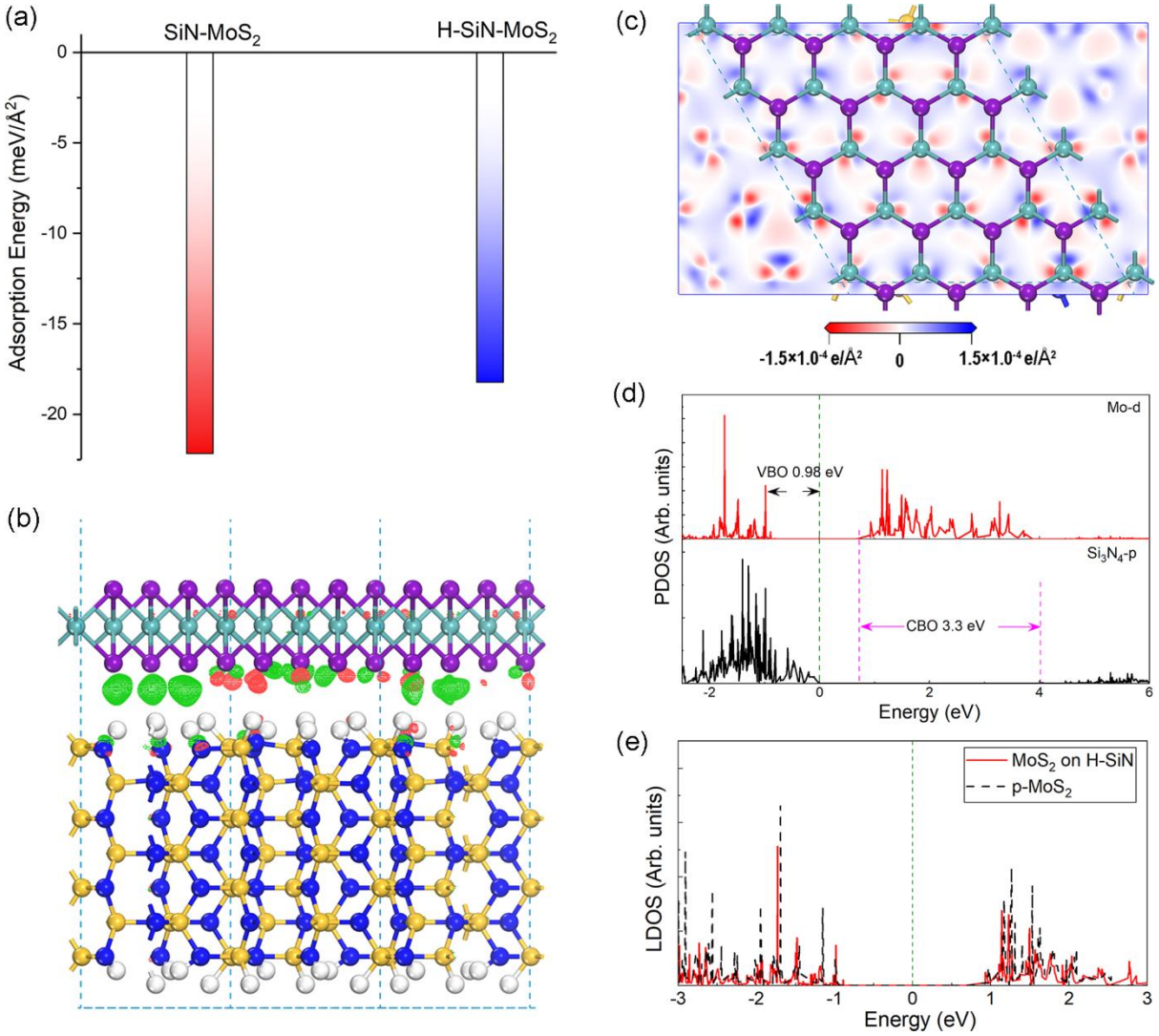

Figure 2. Interface properties of monolayer MoS_2 on hydrogenated β-Si_3N_4 (0001). (a) Adsorption energy of monolayer MoS_2 on β-Si_3N_4 (0001) with or w/o surface hydrogenation. (b) The side view of interface structure for monolayer MoS_2 on hydrogenated β-Si_3N_4 (0001) superimposed with visualized charge density redistribution using an iso-surface value of 1.5×10^{-4} e/Å^3, in which red and green dots denote the depleted and accumulated charge density, respectively. (c) The charge puddles distributed on the Mo plane (top view). (d) The PDOSs on Mo d orbital and p orbitals of central Si_3N_4 layer. (e) LDOSs of MoS_2 monolayer on hydrogenated β-Si_3N_4 (0001) and the pristine monolayer MoS_2.

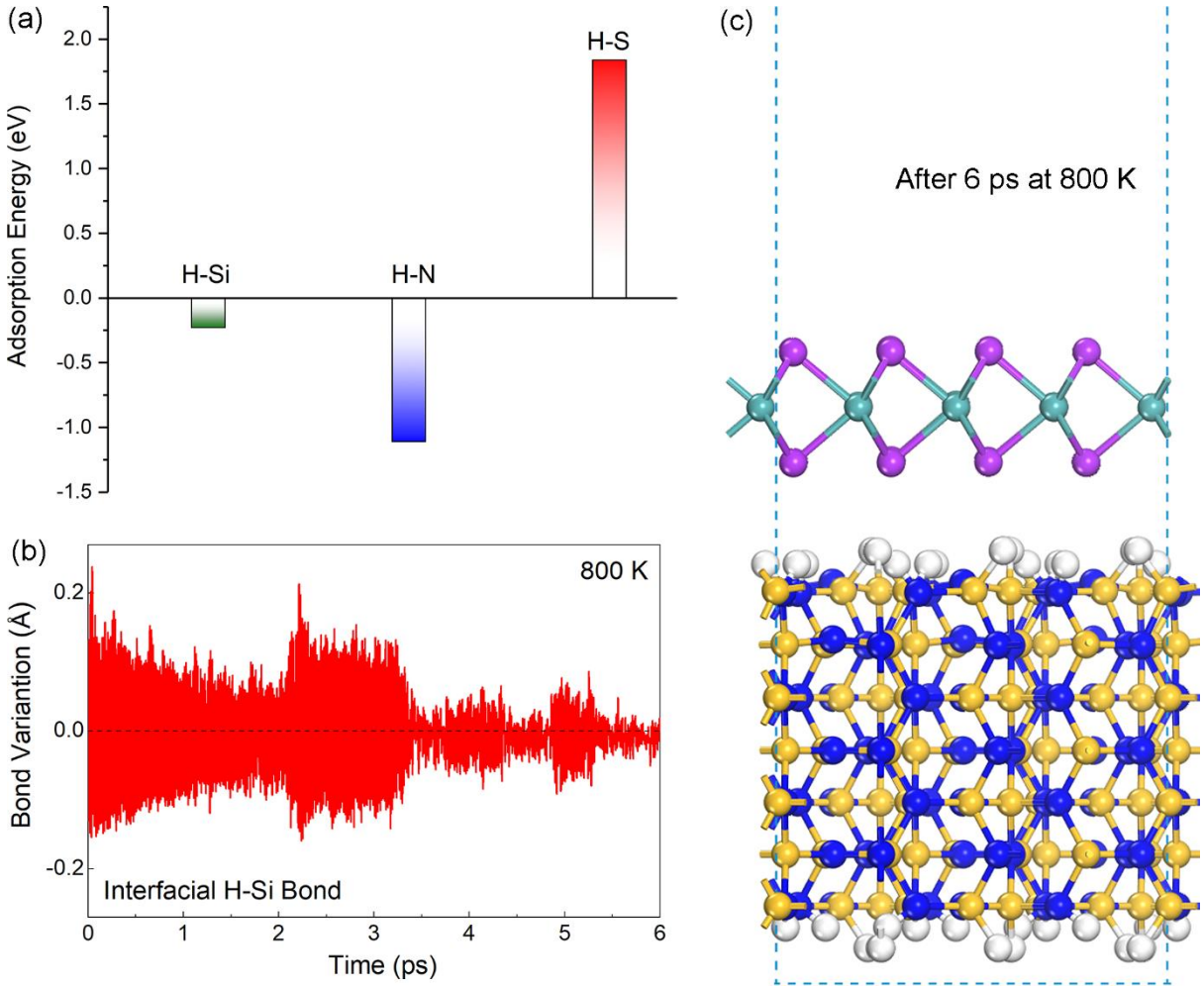

Figure 3. Hydrogenation selectivity and stability. (a) The hydrogen adsorption energy on β-Si_3N_4 (0001) and monolayer MoS_2. (b) The interface Si-H bond variation during the molecular dynamic (MD) simulation at the temperature of 800 K. (c) The final atomic structure (side view) of MoS_2 monolayer on the hydrogenated β-Si_3N_4 (0001) surface after the 6 ps MD simulation.

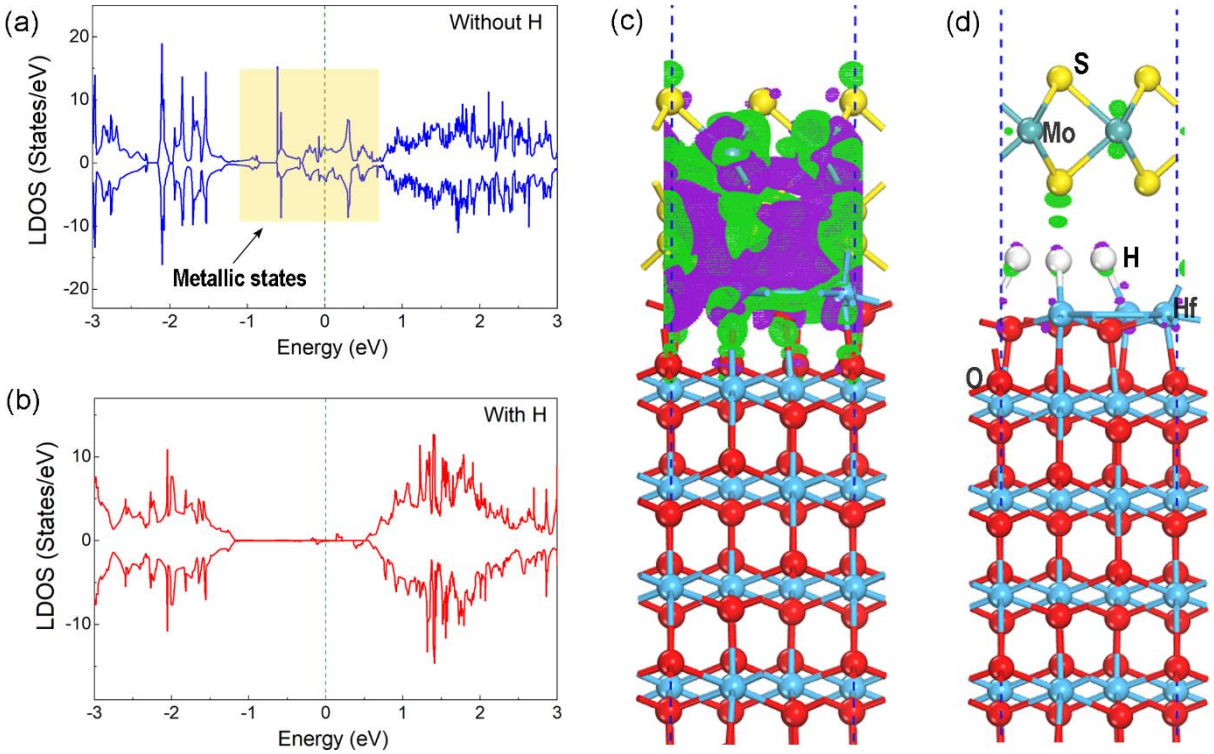

Figure 4. Hydrogenation effect on interface properties of monolayer MoS_2 on Hf-terminated HfO_2 (0001) surface. The LDOSs of MoS_2 monolayer on (a) HfO_2 (0001) surface and (b) hydrogen passivated HfO_2 (0001) surface. The charge density redistribution for MoS_2 monolayer on (ac) HfO_2 (0001) surface and (d) hydrogen passivated HfO_2 (0001) surface, where the green and purple dots denote the excess and accumulated charge density visualized by an iso-surface value of 3.0×10^{-3} e/Å^3, respectively.

References

[1] Fiori, G.;Bonaccorso, F.;Iannaccone, G.;Palacios, T.;Neumaier, D.;Seabaugh, A.;Banerjee, S. K.; Colombo, L. Electronics based on two-dimensional materials. *Nat. Nanotechnol.* **2014**, *9*, 768-779.

[2] Li, M.-Y.;Su, S.-K.;Wong, H.-S. P.; Li, L.-J. How 2D semiconductors could extend Moore's law. *Nature* **2019**, *567*, 169-170.

[3] Mak, K. F.;Lee, C.;Hone, J.;Shan, J.; Heinz, T. F. Atomically thin MoS_2: a new direct-gap semiconductor. *Phys. Rev. Lett.* **2010**, *105*, 136805.

[4] Butler, S. Z.;Hollen, S. M.;Cao, L.;Cui, Y.;Gupta, J. A.;Gutiérrez, H. R.;Heinz, T. F.;Hong, S. S.;Huang, J.; Ismach, A. F. Progress, challenges, and opportunities in two-dimensional materials beyond graphene. *ACS Nano* **2013**, *7*, 2898-2926.

[5] Yoon, Y.;Ganapathi, K.; Salahuddin, S. How good can monolayer MoS_2 transistors be? *Nano Lett.* **2011**, *11*, 3768-3773.

[6] Wang, G.;Chernikov, A.;Glazov, M. M.;Heinz, T. F.;Marie, X.;Amand, T.; Urbaszek, B. Colloquium: Excitons in atomically thin transition metal dichalcogenides. *Rev. Mod. Phys.* **2018**, *90*, 021001.

[7] Liu, G.-B.;Xiao, D.;Yao, Y.;Xu, X.; Yao, W. Electronic structures and theoretical modelling of two-dimensional group-VIB transition metal dichalcogenides. *Chem. Soc. Rev.* **2015**, *44*, 2643-2663.

[8] Wang, Q. H.;Kalantar-Zadeh, K.;Kis, A.;Coleman, J. N.; Strano, M. S. Electronics and optoelectronics of two-dimensional transition metal dichalcogenides. *Nat. Nanotechnol.* **2012**, *7*, 699-712.

[9] Novoselov, K. S.;Jiang, D.;Schedin, F.;Booth, T.;Khotkevich, V.;Morozov, S.; Geim, A. K. Two-dimensional atomic crystals. *Proc. Natl. Acad. Sci. U.S.A.* **2005**, *102*, 10451-10453.

[10] Sangwan, V. K.;Lee, H.-S.;Bergeron, H.;Balla, I.;Beck, M. E.;Chen, K.-S.; Hersam, M. C. Multi-terminal memtransistors from polycrystalline monolayer molybdenum disulfide. *Nature* **2018**, *554*, 500-504.

[11] Chenqiang, H.;Hua, B.;Yi, Z.;Zhu-An, X.;Shengyuan, A. Y.;Yunhao, L.; Su-Huai, W. Strong Coupled Magnetic and Electric Ordering in Monolayer of Metal Thio (seleno) phosphates. *Chin. Phys. Lett.* **2021**, *38*, 77501-077501.

[12] Bai, H.;Wang, X.;Wu, W.;He, P.;Yang, S. A.; Lu, Y. Nonvolatile ferroelectric control of topological states in two-dimensional heterostructures. *Phys. Rev. B* **2020**, *102*, 235403.

[13] Wang, X.;Xiao, C.;Yang, C.;Chen, M.;Yang, S. A.;Hu, J.;Ren, Z.;Pan, H.;Zhu, W.; Xu, Z.-A. Ferroelectric control of single-molecule magnetism in 2D limit. *Sci. Bull.* **2020**, *65*, 1252-1259.

[14] Radisavljevic, B.;Radenovic, A.;Brivio, J.;Giacometti, V.; Kis, A. Single-layer MoS_2 transistors. *Nat. Nanotechnol.* **2011**, *6*, 147-150.

[15] Kim, S.;Konar, A.;Hwang, W.-S.;Lee, J. H.;Lee, J.;Yang, J.;Jung, C.;Kim, H.;Yoo, J.-B.; Choi, J.-Y. High-mobility and low-power thin-film transistors based on multilayer MoS_2 crystals. *Nat. Commun.* **2012**, *3*, 1-7.

[16] Desai, S. B.;Madhvapathy, S. R.;Sachid, A. B.;Llinas, J. P.;Wang, Q.;Ahn, G. H.;Pitner, G.;Kim, M. J.;Bokor, J.; Hu, C. MoS_2 transistors with 1-nanometer gate lengths. *Science* **2016**, *354*, 99-102.

[17] Briggs, N.;Subramanian, S.;Lin, Z.;Li, X.;Zhang, X.;Zhang, K.;Xiao, K.;Geohegan, D.;Wallace, R.; Chen, L.-Q. A roadmap for electronic grade 2D materials. *2d Mater.* **2019**, *6*, 022001.

[18] Lee, Y. H.;Zhang, X. Q.;Zhang, W.;Chang, M. T.;Lin, C. T.;Chang, K. D.;Yu, Y. C.;Wang, J. T. W.;Chang, C. S.; Li, L. J. Synthesis of large-area MoS_2 atomic layers with chemical vapor deposition. *Adv. Mater.* **2012**, *24*, 2320-2325.

[19] Kang, K.;Xie, S.;Huang, L.;Han, Y.;Huang, P. Y.;Mak, K. F.;Kim, C.-J.;Muller, D.; Park, J. High-mobility three-atom-thick semiconducting films with wafer-scale homogeneity. *Nature* **2015**, *520*, 656-660.

[20] Chai, J.;Tong, S.;Li, C.;Manzano, C.;Li, B.;Liu, Y.;Lin, M.;Wong, L.;Cheng, J.; Wu, J. MoS_2/Polymer Heterostructures Enabling Stable Resistive Switching and Multistate Randomness. *Adv. Mater.* **2020**, *32*, 2002704.

[21] Cai, Z.;Liu, B.;Zou, X.; Cheng, H.-M. Chemical vapor deposition growth and applications of two-dimensional materials and their heterostructures. *Chem. Rev.* **2018**, *118*, 6091-6133.

[22] Lim, Y.-F.;Priyadarshi, K.;Bussolotti, F.;Gogoi, P. K.;Cui, X.;Yang, M.;Pan, J.;Tong, S. W.;Wang, S.; Pennycook, S. J. Modification of vapor phase concentrations in MoS_2 growth using a NiO foam barrier. *ACS Nano* **2018**, *12*, 1339-1349.

[23] Liu, Y.;Guo, J.;Zhu, E.;Liao, L.;Lee, S.-J.;Ding, M.;Shakir, I.;Gambin, V.;Huang, Y.; Duan, X. Approaching the Schottky–Mott limit in van der Waals metal–semiconductor junctions. *Nature* **2018**, *557*, 696-700.

[24] Wang, Y.;Kim, J. C.;Wu, R. J.;Martinez, J.;Song, X.;Yang, J.;Zhao, F.;Mkhoyan, A.;Jeong, H. Y.; Chhowalla, M. Van der Waals contacts between three-dimensional metals and two-dimensional semiconductors. *Nature* **2019**, *568*, 70-74.

[25] Liu, Y.;Stradins, P.; Wei, S.-H. Van der Waals metal-semiconductor junction: Weak Fermi level pinning enables effective tuning of Schottky barrier. *Sci. Adv.* **2016**, *2*, e1600069.

[26] Allain, A.;Kang, J.;Banerjee, K.; Kis, A. Electrical contacts to two-dimensional semiconductors. *Nat. Mater.* **2015**, *14*, 1195-1205.

[27] Shen, P.-C.;Su, C.;Lin, Y.;Chou, A.-S.;Cheng, C.-C.;Park, J.-H.;Chiu, M.-H.;Lu, A.-Y.;Tang, H.-L.; Tavakoli, M. M. Ultralow contact resistance between semimetal and monolayer semiconductors. *Nature* **2021**, *593*, 211-217.

[28] Chai, J. W.;Yang, M.;Callsen, M.;Zhou, J.;Yang, T.;Zhang, Z.;Pan, J. S.;Chi, D. Z.;Feng, Y. P.; Wang, S. J. Tuning contact barrier height between metals and MoS_2 monolayer through interface engineering. *Adv. Mater. Interfaces* **2017**, *4*, 1700035.

[29] Wang, B.;Huang, W.;Chi, L.;Al-Hashimi, M.;Marks, T. J.; Facchetti, A. High-k gate dielectrics for emerging flexible and stretchable electronics. *Chem. Rev.* **2018**, *118*, 5690-5754.

[30] Li, W.;Zhou, J.;Cai, S.;Yu, Z.;Zhang, J.;Fang, N.;Li, T.;Wu, Y.;Chen, T.; Xie, X. Uniform and ultrathin high-κ gate dielectrics for two-dimensional electronic devices. *Nat. Electron.* **2019**, *2*, 563-571.

[31] Illarionov, Y. Y.;Knobloch, T.;Jech, M.;Lanza, M.;Akinwande, D.;Vexler, M. I.;Mueller, T.;Lemme, M. C.;Fiori, G.; Schwierz, F. Insulators for 2D nanoelectronics: the gap to bridge. *Nat. Commun.* **2020**, *11*, 1-15.

[32] Zou, X.;Wang, J.;Chiu, C. H.;Wu, Y.;Xiao, X.;Jiang, C.;Wu, W. W.;Mai, L.;Chen, T.; Li, J. Interface engineering for high-performance top-gated MoS_2 field-effect transistors. *Adv. Mater.* **2014**, *26*, 6255-6261.

[33] Robertson, J. High dielectric constant gate oxides for metal oxide Si transistors. *Rep. Prog. Phys.* **2005**, *69*, 327.

[34] Jena, D.; Konar, A. Enhancement of carrier mobility in semiconductor nanostructures by dielectric engineering. *Phys. Rev. Lett.* **2007**, *98*, 136805.

[35] Lee, G.-H.;Yu, Y.-J.;Cui, X.;Petrone, N.;Lee, C.-H.;Choi, M. S.;Lee, D.-Y.;Lee, C.;Yoo, W. J.; Watanabe, K. Flexible and transparent MoS_2 field-effect transistors on hexagonal boron nitride-graphene heterostructures. *ACS Nano* **2013**, *7*, 7931-7936.

[36] Cui, X.;Lee, G.-H.;Kim, Y. D.;Arefe, G.;Huang, P. Y.;Lee, C.-H.;Chenet, D. A.;Zhang, X.;Wang, L.; Ye, F. Multi-terminal transport measurements of MoS_2 using a van der Waals heterostructure device platform. *Nat. Nanotechnol.* **2015**, *10*, 534-540.

[37] Illarionov, Y. Y.;Banshchikov, A. G.;Polyushkin, D. K.;Wachter, S.;Knobloch, T.;Thesberg, M.;Mennel, L.;Paur, M.;Stöger-Pollach, M.; Steiger-Thirsfeld, A. Ultrathin calcium fluoride insulators for two-dimensional field-effect transistors. *Nat. Electron.* **2019**, *2*, 230-235.

[38] Knobloch, T.;Illarionov, Y. Y.;Ducry, F.;Schleich, C.;Wachter, S.;Watanabe, K.;Taniguchi, T.;Mueller, T.;Waltl, M.; Lanza, M. The performance limits of hexagonal boron nitride as an insulator for scaled CMOS devices based on two-dimensional materials. *Nat. Electron.* **2021**, *4*, 98-108.

[39] McDonnell, S.;Brennan, B.;Azcatl, A.;Lu, N.;Dong, H.;Buie, C.;Kim, J.;Hinkle, C. L.;Kim, M. J.; Wallace, R. M. HfO_2 on MoS_2 by atomic layer deposition: adsorption mechanisms and thickness scalability. *ACS Nano* **2013**, *7*, 10354-10361.

[40] Liu, H.; Peide, D. Y. MoS_2 dual-gate MOSFET with atomic-layer-deposited Al_2O_3 as top-gate dielectric. *IEEE Electron Device Lett.* **2012**, *33*, 546-548.

[41] Kim, H. G.; Lee, H.-B.-R. Atomic layer deposition on 2D materials. *Chem. Mater.* **2017**, *29*, 3809-3826.

[42] Tao, J.;Chai, J.;Zhang, Z.;Pan, J.; Wang, S. The energy-band alignment at molybdenum disulphide and high-k dielectrics interfaces. *Appl. Phys. Lett.* **2014**, *104*, 232110.

[43] Xia, P.;Feng, X.;Ng, R. J.;Wang, S.;Chi, D.;Li, C.;He, Z.;Liu, X.; Ang, K.-W. Impact and origin of interface states in MOS capacitor with monolayer MoS_2 and HfO_2 High-k dielectric. *Sci. Rep.* **2017**, *7*, 1-9.

[44] Pan, Y.;Jia, K.;Huang, K.;Wu, Z.;Bai, G.;Yu, J.;Zhang, Z.;Zhang, Q.; Yin, H. Near-ideal subthreshold swing MoS_2 back-gate transistors with an optimized ultrathin HfO_2 dielectric layer. *Nanotechnology* **2019**, *30*, 095202.

[45] Hu, Y.;San Yip, P.;Tang, C. W.;Lau, K. M.; Li, Q. Interface passivation and trap reduction via hydrogen fluoride for molybdenum disulfide on silicon oxide back-gate transistors. *Semicond. Sci. Technol.* **2018**, *33*, 045005.

[46] Park, J. H.;Fathipour, S.;Kwak, I.;Sardashti, K.;Ahles, C. F.;Wolf, S. F.;Edmonds, M.;Vishwanath, S.;Xing, H. G.; Fullerton-Shirey, S. K. Atomic layer deposition of Al_2O_3 on WSe_2 functionalized by titanyl phthalocyanine. *ACS nano* **2016**, *10*, 6888-6896.

[47] Kresse, G.; Hafner, J. Ab initio molecular dynamics for liquid metals. *Phys. Rev. B* **1993**, *47*, 558.

[48] Perdew, J. P.;Burke, K.; Ernzerhof, M. Generalized gradient approximation made simple. *Phys. Rev. Lett.* **1996**, *77*, 3865.

[49] Blöchl, P. E. Projector augmented-wave method. *Phys. Rev. B* **1994**, *50*, 17953.

[50] Wu, X.;Vargas, M.;Nayak, S.;Lotrich, V.; Scoles, G. Towards extending the applicability of density functional theory to weakly bound systems. *J. Chem. Phys.* **2001**, *115*, 8748-8757.

[51] Yang, M.;Chai, J. W.;Callsen, M.;Zhou, J.;Yang, T.;Song, T. T.;Pan, J. S.;Chi, D. Z.;Feng, Y. P.; Wang, S. J. Interfacial interaction between HfO_2 and MoS_2: from thin films to monolayer. *J. Phys. Chem. C* **2016**, *120*, 9804-9810.

[52] Yang, M.;Zhang, C.;Wang, S.;Feng, Y.; Ariando Graphene on β-Si_3N_4: An ideal system for graphene-based electronics. *AIP Adv.* **2011**, *1*, 032111.

[53] Wang, X.-s.;Zhai, G.;Yang, J.; Cue, N. Crystalline Si_3N_4 thin films on Si (111) and the 4×4 reconstruction on Si_3N_4 (0001). *Phys. Rev. B* **1999**, *60*, R2146.

[54] Yang, M.;Wu, R.;Deng, W.;Shen, L.;Sha, Z.;Cai, Y.;Feng, Y.; Wang, S. Electronic structures of β-Si_3N_4 (0001)/Si (111) interfaces: Perfect bonding and dangling bond effects. *J. Appl. Phys.* **2009**, *105*, 024108.

[55] Bermudez, V. Theoretical study of the electronic structure of the Si_3N_4 (0001) surface. *Surf. Sci.* **2005**, *579*, 11-20.

[56] Bengtsson, L. Dipole correction for surface supercell calculations. *Phys. Rev. B* **1999**, *59*, 12301.

[57] Ma, T. Making silicon nitride film a viable gate dielectric. *IEEE Trans. Electron Devices* **1998**, *45*, 680-690.

[58] Zhu, W.;Neumayer, D.;Perebeinos, V.; Avouris, P. Silicon nitride gate dielectrics and band gap engineering in graphene layers. *Nano Lett.* **2010**, *10*, 3572-3576.

[59] Yang, M.;Chai, J.;Wang, Y.;Wang, S.; Feng, Y. Interfacial properties of silicon nitride grown on epitaxial graphene on 6H-SiC substrate. *J. Phys. Chem. C* **2012**, *116*, 22315-22318.

[60] Huang, B.;Xu, Q.; Wei, S.-H. Theoretical study of corundum as an ideal gate dielectric material for graphene transistors. *Phys. Rev. B* **2011**, *84*, 155406.

[61] Scopel, W.;Miwa, R.;Schmidt, T.; Venezuela, P. MoS_2 on an amorphous HfO_2 surface: An ab initio investigation. *J. Appl. Phys.* **2015**, *117*, 194303.

[62] Kang, Y.-J.;Kang, J.; Chang, K.-J. Electronic structure of graphene and doping effect on SiO_2. *Phys. Rev. B* **2008**, *78*, 115404.

[63] Kamiya, K.;Umezawa, N.; Okada, S. Energetics and electronic structure of graphene adsorbed on HfO_2 (111): Density functional theory calculations. *Phys. Rev. B* **2011**, *83*, 153413.

[64] Dolui, K.;Rungger, I.; Sanvito, S. Origin of the n-type and p-type conductivity of MoS_2 monolayers on a SiO_2 substrate. *Phys. Rev. B* **2013**, *87*, 165402.

[65] Martin, J.;Akerman, N.;Ulbricht, G.;Lohmann, T.;Smet, J. v.;Von Klitzing, K.; Yacoby, A. Observation of electron–hole puddles in graphene using a scanning single-electron transistor. *Nat. Phys.* **2008**, *4*, 144-148.

[66] Ashok, S. Research in Hydrogen Passivation of Defects and Impurities in Silicon: Final Report, 2 May 2000-2 July 2003. National Renewable Energy Lab., Golden, CO (US), 2004.

[67] Yang, T.;Bao, Y.;Xiao, W.;Zhou, J.;Ding, J.;Feng, Y. P.;Loh, K. P.;Yang, M.; Wang, S. J. Hydrogen Evolution Catalyzed by a Molybdenum Sulfide Two-Dimensional Structure with Active Basal Planes. *ACS Appl. Mater. Interfaces* **2018**, *10*, 22042-22049.

[68] Sze, S. M. *Semiconductor devices: physics and technology*; John wiley & sons, 2008.

[69] Liu, H.;Xu, K.;Zhang, X.; Ye, P. D. The integration of high-k dielectric on two-dimensional crystals by atomic layer deposition. *Appl. Phys. Lett.* **2012**, *100*, 152115.

[70] Hausmann, D. M.;Kim, E.;Becker, J.; Gordon, R. G. Atomic layer deposition of hafnium and zirconium oxides using metal amide precursors. *Chem. Mater.* **2002**, *14*, 4350-4358.

[71] Liu, X.;Ramanathan, S.;Longdergan, A.;Srivastava, A.;Lee, E.;Seidel, T. E.;Barton, J. T.;Pang, D.; Gordon, R. G. ALD of hafnium oxide thin films from tetrakis (ethylmethylamino) hafnium and ozone. *J. Electrochem. Soc.* **2005**, *152*, G213.

[72] Yang, M.;Nurbawono, A.;Zhang, C.;Feng, Y. P.; Ariando Two-dimensional graphene superlattice made with partial hydrogenation. *Appl. Phys. Lett.* **2010**, *96*, 193115.

[73] Rahman, M. Z.;Kwong, C. W.;Davey, K.; Qiao, S. Z. 2D phosphorene as a water splitting photocatalyst: fundamentals to applications. *Energy Environ. Sci.* **2016**, *9*, 709-728.